Accepted Manuscript

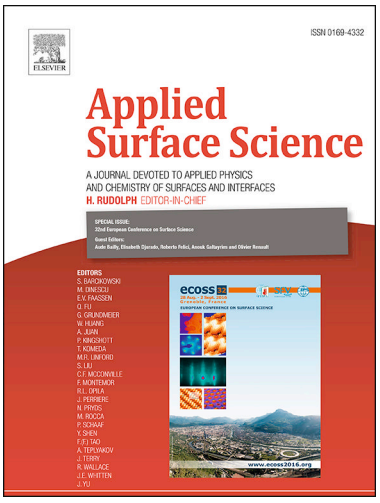

Full Length Article

In situ phase transformation synthesis of unique Janus Ag_2O/Ag_2CO_3 hetero-junction photocatalyst with improved photocatalytic properties

Wan-Kuen Jo, Santosh Kumar, Poonam Yadav, Surendar Tonda

PII: S0169-4332(18)30880-8
DOI: https://doi.org/10.1016/j.apsusc.2018.03.194
Reference: APSUSC 38942

To appear in: *Applied Surface Science*

Received Date: 6 February 2018
Revised Date: 21 March 2018
Accepted Date: 24 March 2018

Please cite this article as: W-K. Jo, S. Kumar, P. Yadav, S. Tonda, In situ phase transformation synthesis of unique Janus Ag_2O/Ag_2CO_3 heterojunction photocatalyst with improved photocatalytic properties, *Applied Surface Science* (2018), doi: https://doi.org/10.1016/j.apsusc.2018.03.194

In situ phase transformation synthesis of unique Janus Ag_2O/Ag_2CO_3 heterojunction photocatalyst with improved photocatalytic properties

Wan-Kuen Jo,[a] Santosh Kumar,[b] Poonam Yadav,[c] Surendar Tonda [a,*]

[a]Department of Environmental Engineering, Kyungpook National University, Daegu 702-701, South Korea.

[b]European Bioenergy Research Institute, Aston University, Birmingham B4 7ET, UK.

[c]Physical and Materials Chemistry Division, National Chemical Laboratory (CSIR-NCL), Pashan, Pune 411008, India.

*Corresponding Author:
E-mail: surendar.t86@gmail.com; surendart@knu.ac.kr
Contact No.: +82 53 950 6584.

Abstract

Herein, Ag_2O/Ag_2CO_3 nanocomposite with unique Janus morphology was synthesized by a facile ion-exchange followed by an in situ phase transformation method with precise control of its nucleation and growth processes. Contrary to conventional synthetic procedures of Janus architectures, the present Janus system was constructed without the need for surfactants or toxic chemicals. Most importantly, the visible-light-absorbing Janus Ag_2O/Ag_2CO_3 nanocomposite exhibits a remarkable performance toward the degradation of Rhodamine B and 4-chlorophenol, far superior to that observed for bare Ag_2CO_3. The obvious enhancement of the photocatalytic performance of this nanocomposite is mainly attributed to the intimate Ag_2O/Ag_2CO_3 interface created by its exceptional Janus architecture, which in turn allows for rapid charge transfer processes. Additionally, the Janus system exhibited a high photostability during recycling experiments with no significant change in the degradation activity.

Keywords: Janus structure; photocatalysis; Ag_2CO_3; heterojunction; interface

1. Introduction

The rapid consumption of fossil-fuel stocks driven by the ever-growing world population has created significant challenges to modern-day researchers regarding alternative energy sources and their related environmental issues. Solar energy is a clean and abundant energy source, and its conversion into usable energy through photocatalysis technologies has been regarded as one of the most promising approaches to meet the future energy requirements and resolve the associated environmental problems [1-6]. For such purposes, a wide range of semiconductors, such as TiO_2, ZnO, etc., has been extensively investigated in the past few decades [7,8]. However, most of them still suffer from low quantum yields and UV-only absorption (ca. 4% of the solar spectrum), which greatly limit their practical implementation for solar energy conversion. Therefore, vast efforts have been devoted to the design and exploration of visible-light-active photocatalysts able to efficiently harness a wider range of the solar spectrum.

Silver-based semiconductor materials have emerged as promising photocatalysts owing to their excellent response to visible light [9-15]. To date, various Ag-based materials, such as Ag_3PO_4, Ag_3VO_4, Ag_2CO_3, AgCl, and $AgSbO_3$, have been studied for diverse photocatalytic applications [16-24]. Among them, Ag_2CO_3 has been recognized as the most promising photocatalyst for the efficient degradation of a variety of organic contaminants when exposed to visible light [25-29]. Nevertheless, Ag_2CO_3 suffers from severe photocorrosion during photocatalysis processes, resulting in severe deactivation during recycling experiments and thus hampering its practical application. To overcome this drawback, the construction of heterojunctions by coupling Ag_2CO_3 with other semiconductors with suitable band potentials has been found to be an effective strategy to improve its photocatalytic performance and photostability [30]. Some researchers have investigated Ag_2CO_3–based coupled photocatalysts,

and provided some insights into important issues that need to be addressed by further work [31-36]. For instance, Yu et al. [30] have reported an Ag_2O/Ag_2CO_3 heterostructure prepared by a phase transformation method and their results have indicated that the heterostructure interface is able to effectively hamper the recombination of photogenerated electrons and holes, leading to enhanced photocatalytic activity and stability. Very recently, Zhao et al. [37] have reported Ag_2O/Ag_2CO_3 3-D hollow flower-like hierarchical microspheres, exhibiting improved photocatalytic performance and stability compared to those of bare Ag_2CO_3. Therefore, there has been great interest in design and development of tunable size and morphology based Ag_2O/Ag_2CO_3 heterostructure for efficient interface contact and charge separation in order to boost the photocatalytic performance and photostability.

In this study, we report for the first time an Ag_2O/Ag_2CO_3 nanocomposite with unique Janus morphology prepared by a facile ion-exchange followed by an in situ phase transformation method with precise control of the nucleation and growth processes. Contrary to conventional synthetic procedures [38,39], the present Janus system does not require the addition of any surfactant or toxic chemical. The photocatalytic performance of the synthesized Janus Ag_2O/Ag_2CO_3 nanocomposites was assessed by the photodegradation of aqueous 4-chlorophenol (4-CP) and Rhodamine B (RhB) contaminants under visible-light irradiation. Moreover, the significance of the Janus morphology on the degradation performance of the present system was systematically investigated, and a possible mechanism for the improved photodegradation performance was proposed based on the findings of trapping, photoluminescence, and photocurrent experiments. Very interestingly, the Ag_2O/Ag_2CO_3 nanocomposites with unique Janus contact showed improved charge separation followed photocatalytic performance and photostability. This facile synthetic method could be expended to prepare various Ag-based

Janus heterostructures for efficient photocatalysis including pollutant degradation, water splitting and CO_2 reduction for sustainable energy and environmental technology.

2. Experimental section

2.1. Materials and method

Silver nitrate, sodium bicarbonate, Rhodamine B, 4-chlorophenol, ammonium oxalate, *tert*-butyl alcohol, and benzoquinone were obtained from Sigma-Aldrich. All the chemicals in this work were used as received without further purification.

The Janus Ag_2O/Ag_2CO_3 nanocomposite was synthesized by a facile ion-exchange followed by an in situ phase transformation method. The detailed procedure is as follows. Silver nitrate (0.0425 g) was first dissolved in 50 mL of a water/ethanol mixture and the reaction solution was then heated to 60 °C. Subsequently, 50 mL of an equimolar solution of sodium bicarbonate was slowly added under constant stirring. After complete addition of the sodium bicarbonate solution, the reaction mixture was refluxed at 80 °C under constant stirring. During this period, the color of the reaction mixture turned from yellow-green to grey. The whole reaction process was completed in approximately 6 h. Once the reaction mixture turned grey, the precipitate was immediately collected by centrifugation, washed with deionized water several times, and dried in an oven at 60 °C for 12 h. Bare Ag_2CO_3 was obtained by a simple room temperature ion-exchange method using the above mentioned concentrations of silver nitrate and sodium bicarbonate solutions. The resulting yellow-green precipitate obtained after 12 h of reaction was collected; this sample was denoted as bare Ag_2CO_3.

Ag_2O was used as the reference material in the present study and synthesized as follows. Silver nitrate (0.21 g) was dissolved in 50 mL of deionized water, and then 50 mL of 0.5 M

NaOH was added drop wise to the solution to adjust the pH to 12. After stirring for 30 min, the obtained black colored precipitate was collected by centrifugation, washed with water and ethanol, and dried at 60 °C.

2.2. Material characterization

The morphology and microstructure of the synthesized catalysts were examined by field-emission transmission electron microscopy (FETEM, FEI Company, Titan G2 ChemiSTEM Cs Probe). The X-ray diffraction (XRD) spectra of the catalysts were recorded on a Rigaku (D/Max-2500) diffractometer with Cu K_α radiation (λ = 1.5408 nm). Time resolved photoluminescence (PL) spectra were obtained on a SHIMADZU RF-6000 spectrofluorophotometer at an excitation wavelength of 400 nm. A SHIMADZU UV-2600 UV-vis spectrophotometer was used to obtain the UV−vis diffuse reflectance spectra (DRS) of the samples. Nitrogen adsorption and desorption isotherm measurements were performed on a BELSORP-max, Japan, apparatus at liquid N_2 temperature. The surface electronic states of the samples were determined using a Thermo Scientific K-Alpha X-ray photoelectron spectrometer. The transient photocurrent measurements were conducted using an IVIUM Technologies electrochemical workstation using a conventional three-electrode system. Ag/AgCl (in saturated KCl) and platinum foil served as the reference and counter electrodes, respectively, and the photocatalyst deposited on indium tin oxide (ITO) as the working electrode. A 300 W Xe lamp was served as the light source and a 0.5 M Na_2SO_4 aqueous solution as the supporting electrolyte. To prepare the working electrode, ~15 mg of the as-synthesized catalyst was suspended in 20 µL of Nafion (5 wt%) and 0.5 mL of ethanol, which was then ground thoroughly to obtain a fine paste. The paste was then evenly spread as a thin film on an ITO glass substrate with an active area of 1.0 cm^2, and the resulting ITO electrodes were dried in an oven at 80 °C.

2.3. Photocatalytic performance testing

The photocatalytic activity of the prepared catalysts was assessed by the photodegradation of aqueous organic contaminants, such as RhB (a widely used hazardous dye) and 4-CP (a colorless water pollutant), under the visible-light illumination provided by a 300 W halogen lamp. The experiments were conducted as follows: 50 mg of the catalyst powder was suspended in 200 mL of an aqueous RhB or 4-CP (5 mg L^{-1}) solution by magnetic stirring. The suspension was magnetically agitated for 30 min in the dark to achieve adsorption/desorption equilibrium between the pollutant and catalyst before light illumination. At defined irradiation time intervals, 3 mL of the suspension was sampled and filtered to remove the catalyst particles. Then, the degradation of the model pollutant was examined by measuring its absorbance at the maximum absorption wavelength on a SHIMADZU UV-2600 UV-Vis spectrophotometer. Control experiments in the absence of catalyst (i.e., photolysis) were also conducted on aqueous solutions of RhB and 4-CP to analyze their intrinsic stability under visible-light illumination. Additionally, to explore the role of the reactive species generated during the photodegradation process, a series of experiments were performed in a similar manner to the photodegradation experiments but with the introduction of different scavengers to the reaction system.

3. Results and discussion

3.1. Photocatalyst morphology and structure characterization

The morphology of the synthesized catalysts was first characterized by TEM. As displayed in Fig. S1, the bare Ag_2CO_3 nanoparticles display spherical-like morphology with an average diameter of 15 nm. Figure 1a clearly shows the Janus morphology of the Ag_2O/Ag_2CO_3 nanocomposite, in particular its acorn-like structural features, which essentially consist of two

different kinds of nanoparticles. The darkest ones are assigned to Ag_2CO_3 nanoparticles, whereas the lighter ones correspond to Ag_2O nanoparticles (Fig. 1b). It is worth noting that the size of the Ag_2CO_3 nanoparticles observed in the Janus nanocomposite is rather smaller than that of the bare Ag_2CO_3 particles (Fig. S2), clearly indicating the in situ formation of the Janus nanocomposite. Moreover, Fig. 1c clearly illustrates the strong coupling between Ag_2CO_3 and Ag_2O in the Janus nanocomposite. In addition, FETEM analysis of the Janus nanocomposite (Fig. 1d) revealed lattice fringes *d*-spaced by 0.23 and 0.27 nm, consistent with the Ag_2CO_3 (031) and Ag_2O (111) diffraction planes, respectively [37,40].

The phase structure and purity of the synthesized bare Ag_2CO_3 and Janus nanocomposite were examined by XRD measurements, and the results are shown in Fig. 2. For comparison, the XRD pattern of Ag_2O is also included. All the diffraction peaks of bare Ag_2CO_3 match well those of the monoclinic phase of Ag_2CO_3 (JCPDS No. 26-0339), while all the diffraction peaks of Ag_2O correspond to cubic phase Ag_2O (JCPDS No. 41-1104). Notably, the XRD pattern of the Janus Ag_2O/Ag_2CO_3 nanocomposite comprises a combination of both the Ag_2CO_3 and Ag_2O peaks; moreover, no other XRD peaks related to impurities can be discerned, indicating the successful fabrication of the Janus nanocomposite.

A comparison of the UV-Vis DRS of the synthesized samples is presented in Fig. 3. The absorption band-edge of bare Ag_2CO_3 extends from the UV to the visible region, corresponding to a band gap of 2.32 eV, consistent with previously reported data [20,37]. Importantly, an obvious improvement of the absorbance in the entire visible-light region is observed for the Janus nanocomposite when compared to the bare Ag_2CO_3 absorption spectrum. The strong visible-light absorption of the Janus nanocomposite will therefore generate a larger number of the charge carriers needed for the photocatalytic reaction, subsequently boosting its

photocatalytic activity. In addition, compared to bare Ag_2CO_3 and the Janus nanocomposite, the reference Ag_2O sample was found to display a higher response to visible light owing to its very low band gap.

The specific surface areas of bare Ag_2CO_3 and the Janus Ag_2O/Ag_2CO_3 nanocomposite were analyzed by nitrogen adsorption-desorption isotherm analysis (Fig. S3). It was found that the specific surface area of the Janus Ag_2O/Ag_2CO_3 nanocomposite (38.5 $m^2\ g^{-1}$) was relatively higher than that of bare Ag_2CO_3 (32.8 $m^2\ g^{-1}$). The high specific surface area of this Janus nanocomposite benefits the better adsorption of pollutants and also provides more reactive sites for the degradation process, thereby improving the photocatalytic activity [41,42].

The surface composition and chemical state of the elements in the synthesized samples were analyzed by XPS. As displayed in Fig. 4a, the pair of symmetric peaks centered at binding energy (BE) values of 367.8 and 373.8 eV was attributed to the $3d_{5/2}$ and $3d_{3/2}$ orbitals of Ag^+ in the Janus nanocomposite [43,44]. A similar pair of Ag 3d peaks was also observed in the bare Ag_2CO_3 and Ag_2O samples, indicating that no metallic silver (Ag^0) was present in any of the synthesized samples. The O 1s peak at BE = 531.2 eV could be attributed to the oxygen atoms in Ag_2CO_3, whereas the peak at 529.6 eV corresponds to the oxygen in Ag_2O (Fig. 4b) [25,45]. Similar chemical states of oxygen in the O 1s spectrum of the Janus nanocomposite clearly evidence the presence of both Ag_2CO_3 and Ag_2O in the nanocomposite. These results are well consistent with the data reported by Yu et al. for an Ag_2O/Ag_2CO_3 composite [30].

Based on the above findings, the following formation mechanism for the Janus Ag_2CO_3/Ag_2O nanocomposite is proposed. When the aqueous sodium bicarbonate is added drop wise to the silver nitrate solution at 60 °C, the reaction solution initially becomes yellow in color, possibly

due to the formation of the weak acid H_2CO_3. During the reaction, the color of the mixture changes into yellow-green upon further addition of sodium bicarbonate, indicating the formation of Ag_2CO_3 by an ion-exchange route (Eq. 1). Under the same conditions, the color of the reaction mixture further changes slowly to grey, as a result of Ag_2CO_3 being further converted into Ag_2O (Eq. 2). This eventually leads to the formation of the acorn-like Janus Ag_2O/Ag_2CO_3 nanocomposite, comprising spherical Ag_2CO_3 on one side and Ag_2O on the other side (as shown in the TEM images). In this synthetic approach, the nucleation and growth processes are finely controlled by the use of very dilute precursors in a water/ethanol mixture and by maintaining a suitable temperature throughout the experiment. The possible reactions in the present synthetic process are summarized by the following equations:

$$2\,AgNO_3 + 2\,NaHCO_3 \rightarrow Ag_2CO_3 + 2\,NaNO_3 + H_2CO_3 \quad (1)$$

$$Ag_2CO_3 + 2\,H_2O \rightarrow Ag_2O + H_2CO_3 + H_2O\,(\text{partial}) \quad (2)$$

3.2. Photocatalytic performance

The photocatalytic activity of the prepared Janus nanocomposite was assessed for the degradation of aqueous RhB and 4-CP under visible-light illumination. Controlled tests in the absence of the catalyst or light illumination were also performed, and the results disclosed that both the catalyst and light illumination are essential to drive the photodegradation process. Figure 5a displays the degradation of RhB as a function of the illumination time over bare Ag_2CO_3 and the Janus nanocomposite. For comparison, the RhB photodegradation performance of Ag_2O and P25 are also included. It can be seen from Fig. 5a that the Janus nanocomposite exhibits a superior photocatalytic performance than bare Ag_2CO_3 and Ag_2O. Almost 99% RhB was degraded over the Janus nanocomposite after 60 min of visible-light illumination, whereas

only 42% and 57% of RhB degradation was achieved over bare Ag_2CO_3 and Ag_2O, respectively, for the same period of light illumination. P25 was found to exhibit the lowest RhB degradation activity among all the tested samples, with which only 28% RhB was degraded after 60 min of visible-light irradiation, possibly due to its UV-light-only absorption and rapid charge carrier recombination. The pseudo-first-order reaction kinetics of the photodegradation of RhB was explored and the results are shown in Fig. 5b. Clearly, the Janus nanocomposite exhibits the highest RhB degradation rate (0.0555 min^{-1}), which is almost 6-, 4-, and 10-times higher than that of bare Ag_2CO_3 (0.0089 min^{-1}), Ag_2O (0.0142 min^{-1}), and P25 (0.0056 min^{-1}), respectively. Furthermore, Fig. 6a shows the degradation of 4-CP over all the synthesized catalysts under visible-light irradiation. Among all the catalysts, the Janus nanocomposite displays the highest degradation performance, with which ~90% of 4-CP was degraded after 180 min of visible-light illumination. However, only 43%, 35%, and 10% of 4-CP was degraded under similar experimental conditions over bare Ag_2CO_3, Ag_2O, and P25, respectively. According to the pseudo-first-order reaction kinetic results (Fig. 6b), the Janus nanocomposite exhibits the highest 4-CP degradation rate, which is about 4-, 6-, and 20-times greater than that of Ag_2CO_3, Ag_2O, and P25, respectively.

The remarkable photodegradation performance of the presented Janus nanocomposite system evidenced an intimate interface between Ag_2CO_3 and Ag_2O, which was further confirmed by the RhB and 4-CP photodegradation results of a physical mixture of Ag_2CO_3 and Ag_2O (termed Ag_2O/Ag_2CO_3 PM in Fig. 5 and 6). Clearly, the physically mixed Ag_2O/Ag_2CO_3 PM composite showed relatively low degradation activities compared to Janus nanocomposite, indicating the absence of strong interactions between Ag_2CO_3 and Ag_2O in the resulting Ag_2O/Ag_2CO_3 PM composite.

Besides the photocatalytic performance, the photostability of silver-based catalysts is a crucial factor for their practical application owing to their well-known serious photocorrosion problems [20,30]. Therefore, to demonstrate the photostability of bare Ag_2CO_3 and the Janus nanocomposite, four successive RhB degradation experiments were carried out under visible-light illumination. As displyed in Fig. 7a, a drastic decrease of the bare Ag_2CO_3 activity was observed in the second run and, by the fourth run, the photocatalyst had lost almost all its activity due to photocorrosion resulting in Ag^0 formation. Remarkably, the Janus nanocomposite retained ca. 90% of its original activity after four consecutive photocatalytic runs, possibly due to no photocorrosion phenomena occurring during the photocatalytic reaction. To confirm this, XPS and XRD analyses were performed on the Janus nanocomposite before and after the photodegradation experimental runs. It can be clearly seen from Fig. S4a that no obvious changes in the BE of Ag 3d exist before and after the photocatalytic runs, clearly indicating that Ag^0 is not formed during the reaction. The XRD patterns of the Janus nanocomposite before and after the photodegradation reactions (Fig. S4b) further confirmed its structural stability even after four successive runs. These results clearly indicate that the Janus nanocomposite is a stable catalyst with great potential for practical applications.

To explore the specific role of primary reactive species in the photodegradation process, trapping experiments were carried out over the Janus nanocomposite under similar experimental conditions to those used above. In this case, three different scavengers, namely, *tert*-butyl alcohol (TBA), benzoquinone (BZQ), and ammonium oxalate (AO), were added to the photocatalytic system to trap $^{\bullet}OH$, $O_2^{\bullet-}$, and h^+, respectively. As shown in Fig. 7b, the RhB photodegradation performance was slightly reduced after the introduction of TBA, indicating that $^{\bullet}OH$ radicals play a minor role in the degradation process. The degradation performance of

Janus nanocomposite was fairly decreased by the addition of BZQ, indicating that $O_2^{\bullet-}$ play a moderate role in the photodegradation reaction. Notably, upon addition of AO, the RhB photodegradation activity of the Janus nanocomposite was extensively suppressed, clearly indicating that h^+ are the primary reactive species involved in the degradation process.

In order to understand the superior photocatalytic performance of the Janus nanocomposite compared to that of bare Ag_2CO_3, a PL spectral analysis was conducted. In general, PL analyses are performed to explore the transfer, migration, and recombination processes of photoinduced electron and holes in semiconductors [41,46]. Since PL emission arises from the recombination of photoinduced charge carriers, lower PL emission intensities indicate lower charge carrier recombination rates. As displayed in Fig. 8a, the PL emission intensity of the Janus nanocomposite is much lower than that of bare Ag_2CO_3, clearly indicating that the recombination of photogenerated electrons and holes is effectively suppressed by the robust heterojunction formed between Ag_2CO_3 and Ag_2O, leading to the improved photocatalytic performance of the Janus nanocomposite. To further confirm the separation efficiency of photoinduced charge carriers in the Janus nanocomposite, transient photocurrent measurements were carried out. As is well known, higher photocurrent responses indicate better electron–hole separation efficiencies [47,48]. Figure 8b displays a comparison of the *I–t* curves for bare Ag_2CO_3 and the Janus nanocomposite with three on–off cycles of intermittent simulated solar-light illumination. Notably, the photocurrent response of the Janus nanocomposite is several times higher than that of bare Ag_2CO_3, indicating a greater separation efficiency of photoinduced charge carriers. This result is well consistent with the PL and photodegradation activity results.

The enhanced photocatalytic performance of the Janus nanocomposite evidences the synergy between the Ag_2CO_3 and Ag_2O components, resulting in improved separation efficiency of the

photogenerated charge carriers. The transfer direction of the photoinduced electrons and holes in the Janus nanocomposite depends on the respective band edge positions of its constituting components. Thus, the band edge positions of Ag_2CO_3 and Ag_2O were determined by valence band XPS measurements (Fig. 9). From valence band XPS results, the valence band (VB) edge potentials of Ag_2CO_3 and Ag_2O were estimated to be +2.65 and +1.42 eV, respectively. Based on the band gap energies of Ag_2CO_3 (2.32 eV) and Ag_2O (1.3 eV) [49,50], the conduction band (CB) edge positions were estimated to be +0.33 and +0.12 eV for Ag_2CO_3 and Ag_2O, respectively. Based on such band edge positions and the above results, a photocatalytic mechanism for the Janus nanocomposite system is proposed in Fig. 10. When the Janus nanocomposite is exposed to visible light, both Ag_2CO_3 and Ag_2O are excited and generate electrons and holes. Due to the intimate interface between Ag_2CO_3 and Ag_2O, the excited electrons in the CB of Ag_2O easily transfer to the CB of Ag_2CO_3, while the holes in the VB of Ag_2CO_3 are also able to migrate to the VB of Ag_2O, thus preventing the photoinduced recombination of electron–hole pairs leading to the observed improved photocatalytic performance. The charge transfer between Ag_2CO_3 and Ag_2O is also facilitated by the CB and VB edge potentials of Ag_2CO_3 being more positive than those of Ag_2O. The accumulated electrons on the surface of Ag_2CO_3 may be trapped by O_2 to generate $O_2^{\bullet-}$, which can further degrade the water pollutants [11,19]. Meanwhile, the accumulated holes on the surface of Ag_2O can also directly degrade the pollutants. On the basis of the aforementioned experimental outcomes, we believe that the robust interface between Ag_2CO_3 and Ag_2O resulting from the Janus morphology of the nanocomposite is able to promote interfacial charge transfer processes and improve the lifetime of the photoinduced charge carriers, imparting enhanced photocatalytic performance and photostability to the Janus nanocomposite.

4. Conclusion

In summary, we have successfully synthesized a Janus Ag_2O/Ag_2CO_3 nanocomposite by a facile ion-exchange followed by an in situ phase transformation method with control of the nucleation and growth processes. The TEM results confirmed the Janus morphology of the nanocomposite. Notably, the synthesized Janus nanocomposite exhibits excellent degradation performance for RhB and 4-CP, much higher than that of bare Ag_2CO_3 as well as Ag_2O and P25 reference materials under visible-light illumination. Trapping experiments confirmed that holes play a major role in the degradation process. The synergistic effect between Ag_2CO_3 and Ag_2O, mainly resulting from the Janus morphology promoting interfacial charge transfer processes and improving the separation efficiency of photoinduced charge carriers, results in the enhanced photocatalytic performance and photostability of such a Janus Ag_2O/Ag_2CO_3 nanocomposite. Therefore, the present work provides insight for the future design of novel Janus catalysts for diverse photocatalytic applications.

Acknowledgements

This work was supported by the National Research Foundation of Korea grant funded by the Korea government (MSIP) (No.2016R1A2B4009122 and No. 2017R1A4A1015628).

References

[1] X. Liu, J. Iocozzia, Y. Wang, X. Cui, Y. Chen, S. Zhao, Z. Li, Z. Lin, Noble metal–metal oxide nanohybrids with tailored nanostructures for efficient solar energy conversion, photocatalysis and environmental remediation, Energy Environ. Sci. 10 (2017) 402–434.

[2] W. Wang, J. Chen, C. Li, W. Tian, Achieving solar overall water splitting with hybrid photosystems of photosystem II and artificial photocatalysts, Nat. Commun. 5 (2014) 4647.

[3] Z. Xiong, Z. Lei, S. Ma, X. Chen, B. Gong, Y. Zhao, J. Zhang, C. Zheng, J.C.S. Wu, Photocatalytic CO_2 reduction over V and W codoped TiO_2 catalyst in an internal-illuminated honeycomb photoreactor under simulated sunlight irradiation, Appl. Catal., B 219 (2017) 412-424.

[4] S. Tonda, S. Kumar, Y. Gawli, M. Bhardwaj, S.B. Ogale, g-C_3N_4 (2D)/CdS (1D)/rGO (2D) dual-interface nano-composite for excellent and stable visible light photocatalytic hydrogen generation, Int. J. Hydrogen Energy 42 (2017) 5971–5984.

[5] J. Wen, J. Xie, X. Chen, X. Li, A review on g-C_3N_4-based photocatalysts, Appl. Surf. Sci. 391 (2017) 72–123.

[6] J. Low, J. Yu, M. Jaroniec, S. Wageh, A.A. Al-Ghamdi, Heterojunction photocatalysts, Adv. Mater. 29 (2017) 1601694.

[7] A. Fujishima, K. Honda, Electrochemical photolysis of water at a semiconductor electrode, Nature 238 (1972) 37–38.

[8] S.T. Kochuveedu, Y.H. Jang, D.H. Kim, A study on the mechanism for the interaction of light with noble metal-metal oxide semiconductor nanostructures for various photophysical applications, Chem. Soc. Rev. 42 (2013) 8467–8493.

[9] C. An, S. Wang, Y. Sun, Q. Zhang, J. Zhang, C. Wang, J. Fang, Plasmonic silver incorporated silver halides for efficient photocatalysis, J. Mater. Chem. A 4 (2016) 4336–4352.

[10] Y. Tang, Z. Jiang, J. Deng, D. Gong, Y. Lai, H. T. Tay, I. T. K. Joo, T. H. Lau, Z. Dong, Z. Chen, Synthesis of nanostructured silver/silver halides on titanate surfaces and their visible-light photocatalytic performance, ACS Appl. Mater. Interfaces 4 (2012) 438−446.

[11] X. Hua, F. Teng, Y. Zhao, J. Xu, C. Xu, Y. Yang, Q. Zhang, S. Paul, Y. Zhang, M. Chen, X. Zhao, A new application of high-efficient silver salts-based photocatalyst under natural indoor weak light for wastewater cleaning, Water Res. 81 (2015) 366–374.

[12] B. Liu, L. Mu, B. Han, J. Zhang, H. Shi, Fabrication of TiO_2/Ag_2O heterostructure with enhanced photocatalytic and antibacterial activities under visible light irradiation, Appl. Surf. Sci. 396 (2017) 1596–1603.

[13] M. Yang, Q. Yang, J. Zhong, S. Huang, J. Li, J. Song, C. Burda, Enhanced photocatalytic performance of Ag_2O/BiOF composite photocatalysts originating from efficient interfacial charge separation, Appl. Surf. Sci. 416 (2017) 666–671.

[14] X. Yang, H. Tang, J. Xu, M. Antonietti, M. Shalom, Silver phosphate/graphitic carbon nitride as an efficient photocatalytic tandem system for oxygen evolution, ChemSusChem 8 (2015) 1350–1358.

[15] H. Yu, W. Chen, X. Wang, Y. Xua, J. Yu, Enhanced photocatalytic activity and photoinduced stability of Ag-based photocatalysts: The synergistic action of amorphous-Ti(IV) and Fe(III) cocatalysts, Appl. Catal., B. 187 (2016) 163–170.

[16] S. Kumar, T. Surendar, A. Baruah, V. Shanker, Synthesis of a novel and stable g-C_3N_4–Ag_3PO_4 hybrid nanocomposite photocatalyst and study of the photocatalytic activity under visible light irradiation, J. Mater. Chem. A 1 (2013) 5333–5340.

[17] Y. Ao, P. Wang, C. Wang, J. Hou, J. Qian, Preparation of graphene oxide–Ag_3PO_4 composite photocatalyst with high visible light photocatalytic activity, Appl. Surf. Sci. 271 (2013) 265–270.

[18] T. Yan, W. Guan, Y. Xiao, J. Tian, Z. Qiao, H. Zhai, W. Li, J. You, Effect of thermal annealing on the microstructures and photocatalytic performance of silver orthophosphate: The synergistic mechanism of Ag vacancies and metallic Ag, Appl. Surf. Sci. 391 (2017) 592–600.

[19] H. Xu, H. Li, L. Xu, C. Wu, G. Sun, Y. Xu, J. Chu, Enhanced photocatalytic activity of Ag_3VO_4 loaded with rare-earth elements under visible-light irradiation, Ind. Eng. Chem. Res. 48 (2009) 10771–10778.

[20] G. Dai, J. Yu, G. Liu, A new approach for photocorrosion inhibition of Ag_2CO_3 photocatalyst with highly visible-light-responsive reactivity, J. Phys. Chem. C 116 (2012) 15519–15524.

[21] A. Zhang, L. Zhang, X. Chen, Q. Zhu, Z. Liu, J. Xiang, Photocatalytic oxidation removal of Hg^0 using ternary Ag/AgI-Ag_2CO_3 hybrids in wet scrubbing process under fluorescent light, Appl. Surf. Sci. 392 (2017) 1107–1116.

[22] X. Wang, S. Li, Y. Ma, H. Yu, J. Yu, $H_2WO_4.H_2O$/Ag/AgCl composite nanoplates: A plasmonic z-scheme visible-light photocatalyst, J. Phys. Chem. C 115 (2011) 14648–14655.

[23] T. Shen, D. Lang, F. Cheng, Q. Xiang, Ternary reduced graphene oxide/g-C_3N_4/Ag-AgCl nanocomposites for controlled visible-light photocatalytic selectivity, ChemistrySelect 5 (2016) 1006–1015.

[24] J. Shi, J. Ye, Q. Li, Z. Zhou, H. Tong, G. Xi, L. Guo, Single-crystal nanosheet-based hierarchical $AgSbO_3$ with exposed {001} facets: topotactic synthesis and enhanced photocatalytic activity, Chem. Eur. J. 18 (2012), 3157–3162.

[25] H. Dong, G. Chen, J. Sun, C. Li, Y. Yu, D. Chen, A novel high-efficiency visible-light sensitive Ag_2CO_3 photocatalyst with universal photodegradation performances: Simple

synthesis, reaction mechanism and first-principles study, Appl. Catal. B Environ. 134–135 (2013) 46–54.

[26] H. Tang, S. Chang, G. Tang, W. Liang, AgBr and g-C_3N_4 co-modified Ag_2CO_3 photocatalyst: A novel multi-heterostructured photocatalyst with enhanced photocatalytic activity, Appl. Surf. Sci. 391 (2017) 440–448.

[27] S. Song, B. Cheng, N. Wu, A. Meng, S. Cao, J. Yu, Structure effect of graphene on the photocatalytic performance of plasmonic Ag/Ag_2CO_3-rGO for photocatalytic elimination of pollutants, Appl. Catal., B. 181 (2016) 71–78.

[28] J. Tian, R. Liu, Z. Liu, C. Yu, M. Liu, Boosting the photocatalytic performance of Ag_2CO_3 crystals in phenol degradation *via* coupling with trace N-CQDs, Chinese J. Catal. 38 (2017) 1999–2008.

[29] W. Wang, Y. Liu, H. Zhang, Y. Qian, Z. Guo, Re-investigation on reduced graphene oxide/Ag_2CO_3 composite photocatalyst: An insight into the double-edged sword role of RGO, Appl. Surf. Sci. 396 (2017) 102–109.

[30] C. Yu, G. Li, S. Kumar, K. Yang, R. Jin, Phase transformation synthesis of novel Ag_2O/Ag_2CO_3 heterostructures with high visible light efficiency in photocatalytic degradation of pollutants, Adv. Mater. 26 (2013) 892–898.

[31] X. Yao, X. Liu, One-pot synthesis of ternary Ag_2CO_3/Ag/AgCl photocatalyst in natural geothermal water with enhanced photocatalytic activity under visible light irradiation, J. Hazard. Mater. 280 (2014) 260–268.

[32] C. Yu, L. Wei, W. Zhou, J. Chen, Q. Fan, H. Liu, Enhancement of the visible light activity and stability of Ag_2CO_3 by formation of AgI/Ag_2CO_3 heterojunction, Appl. Surf. Sci. 319 (2014) 312–318.

[33] Y. Song, J. Zhu, H. Xu, C. Wang, Y. Xu, H. Ji, K. Wang, Q. Zhang, H. Li, Synthesis, characterization and visible-light photocatalytic performance of Ag_2CO_3 modified by graphene-oxide, J. Alloys Compd. 592 (2014) 258–265.

[34] H. Xu, J. Zhu, Y. Song, W. Zhao, Y. Xu, Y. Song, H. Ji, H. Li, Ion-exchange preparation for visible-light-driven photocatalyst AgBr/Ag_2CO_3 and its photocatalytic activity, RSC Adv. 4 (2014) 9139–9147.

[35] C. Dong, K.L. Wu, X.W. Wei, X.Z. Li, L. Liu, T.H. Ding, J. Wang, Y. Ye, Synthesis of graphene oxide–Ag_2CO_3 composites with improved photoactivity and anti-photocorrosion, CrystEngComm 16 (2014) 730–736.

[36] H. Wang, J. Li, P. Huo, Y. Yan, Q. Guan, Preparation of Ag_2O/Ag_2CO_3/MWNTs composite photocatalysts for enhancement of ciprofloxacin degradation, Appl. Surf. Sci. 366 (2016) 1–8.

[37] X. Zhao, Y. Su, X. Qi, X. Han, A facile method to prepare novel Ag_2O/Ag_2CO_3 three-dimensional hollow hierarchical structures and their water purification function, ACS Sustainable Chem. Eng. 5 (2017) 6148–6158.

[38] A. Walther, A.H.E. Muller, Janus particles: synthesis, self-assembly, physical properties, and applications, Chem. Rev. 113 (2013) 5194–5261.

[39] J. Hu, S. Zhou, Y. Sun, X. Fang, L. Wu, Fabrication, properties and applications of Janus particles, Chem. Soc. Rev. 41 (2012) 4356–4378.

[40] X. Yang, R. Li, Y. Wang, K. Wu, S. Chang, H. Tang, Solvent-induced controllable synthesis of recyclable Ag_2CO_3 catalysts with enhanced visible light photocatalytic activity, Ceram. Int. 42 (2016) 13411–13420.

[41] S. Tonda, S. Kumar, S. Kandula, V. Shanker. Fe-doped and -mediated graphitic carbon nitride nanosheets for enhanced photocatalytic performance under natural sunlight, J. Mater. Chem. A 2 (2014) 6772–6780.

[42] D. He, Y. Li, I. Wang, J. Wu, Y. Yang, Q. An, Carbon wrapped and doped TiO_2 mesoporous nanostructure with efficient visible-light photocatalysis for NO removal, Appl. Surf. Sci. 391 (2017) 318–325.

[43] Y. Liu, J. Kong, J. Yuan, W. Zhao, X. Zhu, C. Sun, J. Xie, Enhanced photocatalytic activity over flower-like sphere $Ag/Ag_2CO_3/BiVO_4$ plasmonic heterojunction photocatalyst for tetracycline degradation, Chem. Eng. J. 331 (2018) 242–254.

[44] B.J. Murray, Q. Li, J.T. Newberg, E.J. Menke, J.C. Hemminger, R.M. Penner, Shape- and size-selective electrochemical synthesis of dispersed silver(I) oxide colloids, Nano Lett. 5 (2005) 2319–2324.

[45] J.F. Weaver, G.B. Hoflund, Surface characterization study of the thermal decomposition of Ag_2O, Chem. Mater. 6 (1994), 1693–1699.

[46] W.K. Jo, N.C.S. Selvam, Z-scheme $CdS/g\text{-}C_3N_4$ composites with RGO as an electron mediator for efficient photocatalytic H_2 production and pollutant degradation, Chem. Eng. J. 317 (2017) 913–924.

[47] G. Zhang, C. Huang, X. Wang, Dispersing molecular cobalt in graphitic carbon nitride frameworks for photocatalytic water oxidation, Small 11 (2015) 1215–1221.

[48] S. Tonda, S. Kumar, M. Bhardwaj, P. Yadav, S.B. Ogale, $g\text{-}C_3N_4$/NiAl-LDH 2D/2D hybrid heterojunction for high-performance photocatalytic reduction of CO_2 into renewable fuels, ACS Appl. Mater. Interfaces 10 (2018) 2667–2678.

[49] C. Damm, R. Herrmann, G. Israel, F.W. Muller, Acrylate photopolymerization on heterostructured TiO_2 Photocatalysts, Dyes Pigm. 74 (2007) 335–342.

[50] W. Zhou, H. Liu, J. Wang, D. Liu, G. Du, J. Cui, Ag_2O/TiO_2 nanobelts heterostructure with enhanced ultraviolet and visible photocatalytic activity, ACS Appl. Mater. Interfaces 2 (2010) 2385–2392.

Figure captions

Fig. 1. TEM (a, b) and FETEM (c, d) images of the Janus Ag_2O/Ag_2CO_3 heterojunction.

Fig. 2. XRD patterns of the synthesized bare Ag_2CO_3, Ag_2O, and Janus Ag_2O/Ag_2CO_3 samples.

Fig. 3. UV-vis DRS of bare Ag_2CO_3, Ag_2O, and Janus Ag_2O/Ag_2CO_3 samples.

Fig. 4. High-resolution XPS patterns of Ag 3d and O 1s of the synthesized photocatalysts.

Fig. 5. (a) Comparison of the photocatalytic activities in the decomposition of RhB over the synthesized samples under visible-light illumination, and (b) the related first-order kinetics plots for different samples.

Fig. 6. (a) Comparison of the photocatalytic activities in the decomposition of 4-CP over the synthesized samples under visible-light illumination, and (b) the related first-order kinetics plots for different samples.

Fig. 7. (a) Reusability of the Janus Ag_2O/Ag_2CO_3 nanocomposite for the degradation of RhB upon visible-light over four successive experimental runs. (b) Effects of different scavengers on the degradation of RhB upon visible-light in the presence of the Janus Ag_2O/Ag_2CO_3 nanocomposite.

Fig. 8. (a) Time resolved PL patterns and (b) Photocurrent responses of bare Ag_2CO_3 and Janus Ag_2O/Ag_2CO_3 nanocomposite.

Fig. 9. Valance band XP spectra of bare Ag_2CO_3 and Ag_2O samples.

Fig. 10. Schematic illustration of the charge transfer and separation in the Janus Ag_2O/Ag_2CO_3 heterojunction system under visible-light illumination.

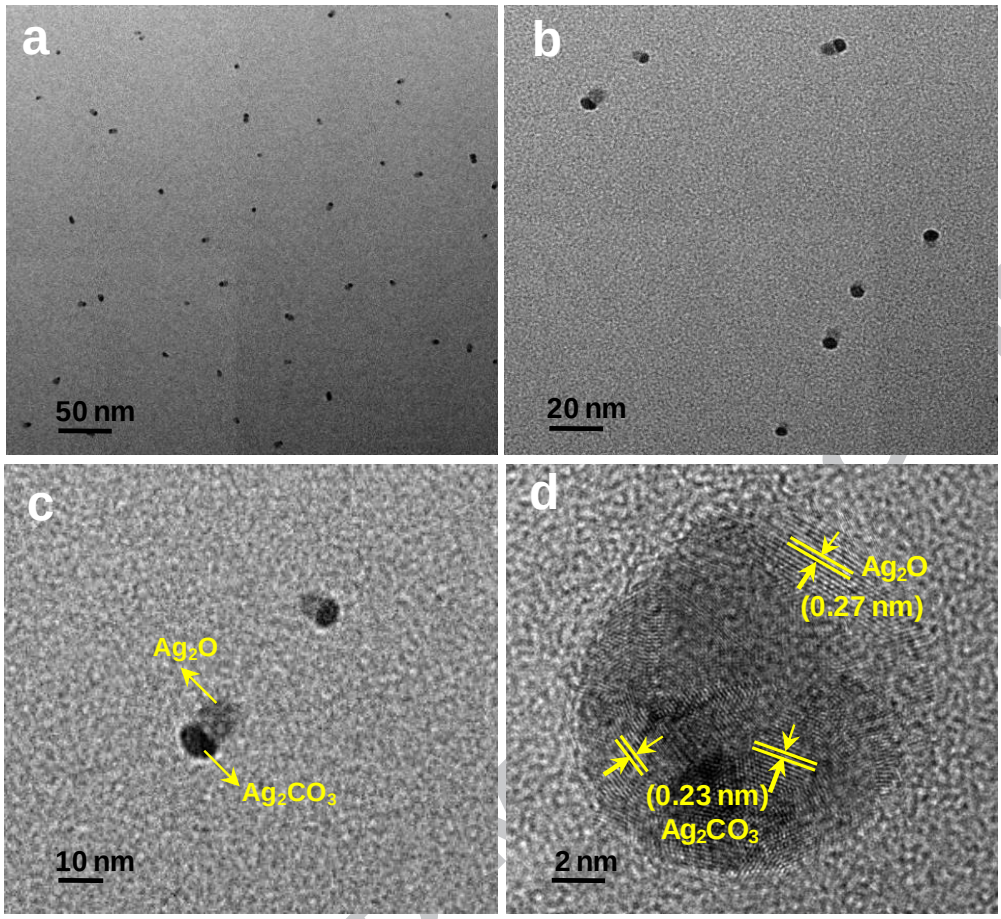

Fig. 1. TEM (a, b) and FETEM (c, d) images of the Janus Ag_2O/Ag_2CO_3 heterojunction.

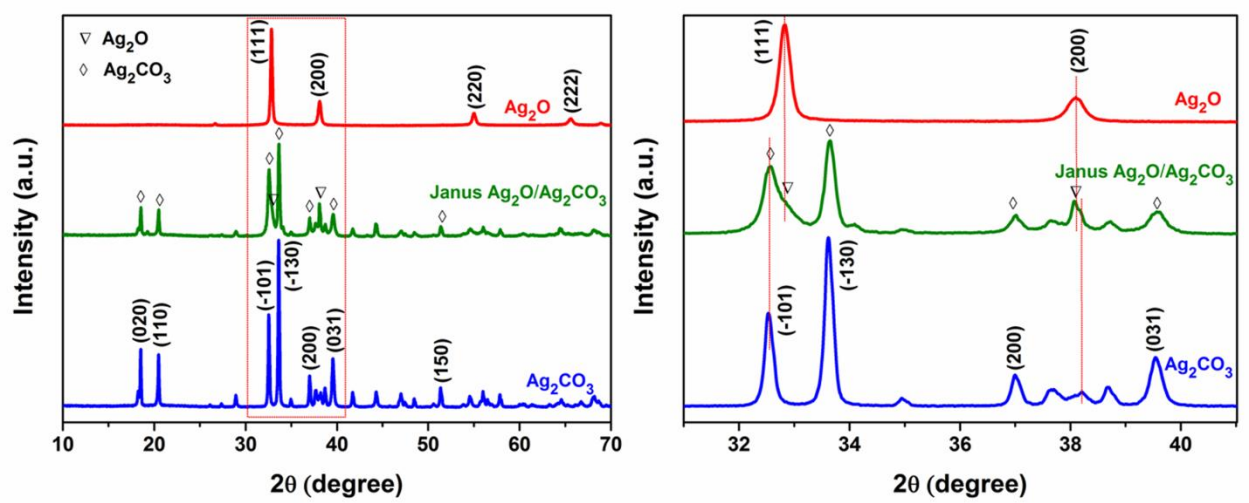

Fig. 2. XRD patterns of the synthesized bare Ag_2CO_3, Ag_2O, and Janus Ag_2O/Ag_2CO_3 samples.

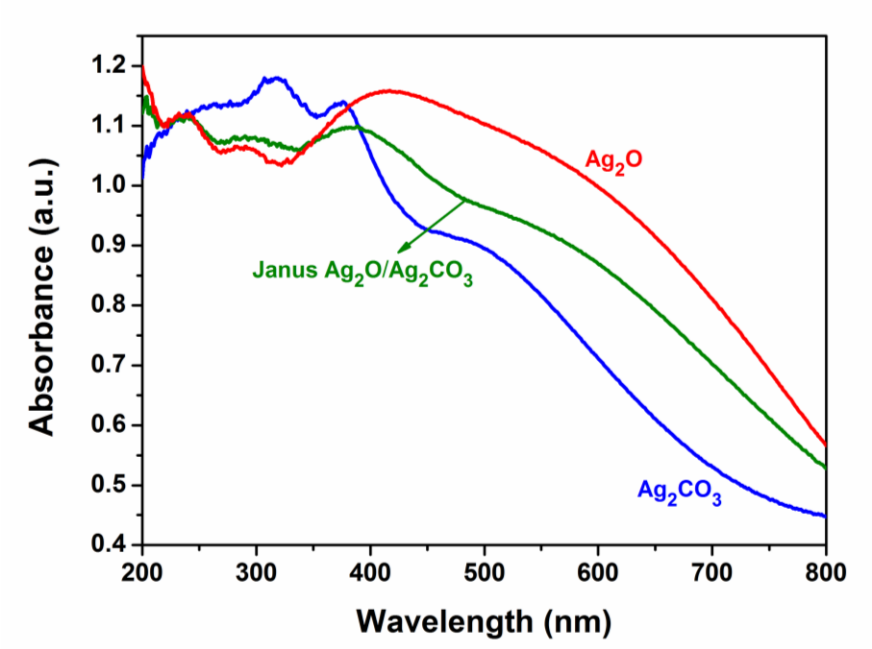

Fig. 3. UV-vis DRS of bare Ag_2CO_3, Ag_2O, and Janus Ag_2O/Ag_2CO_3 samples.

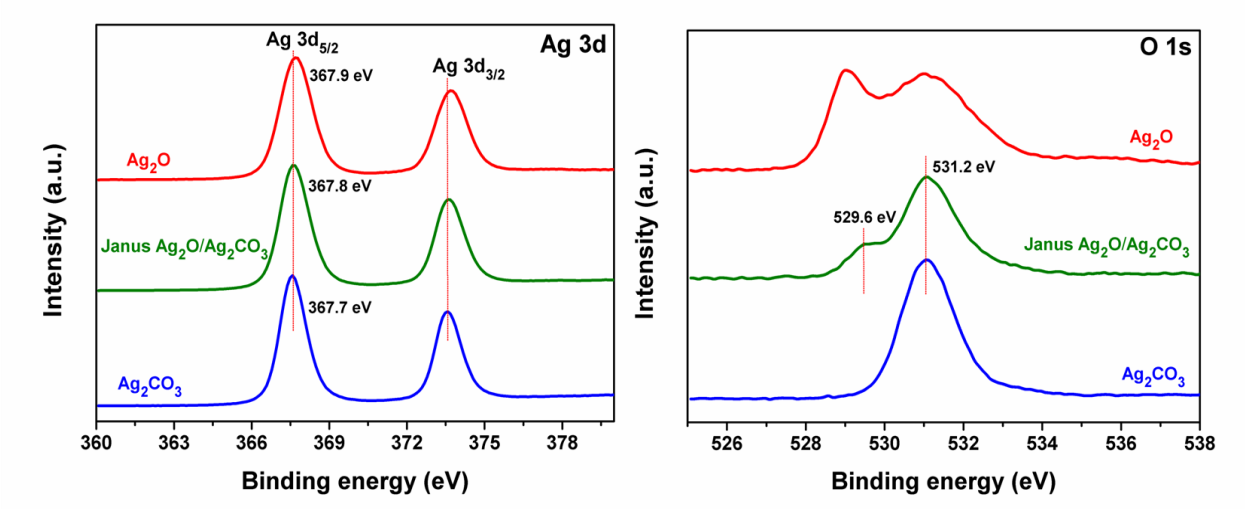

Fig. 4. High-resolution XPS patterns of Ag 3d and O 1s of the synthesized photocatalysts.

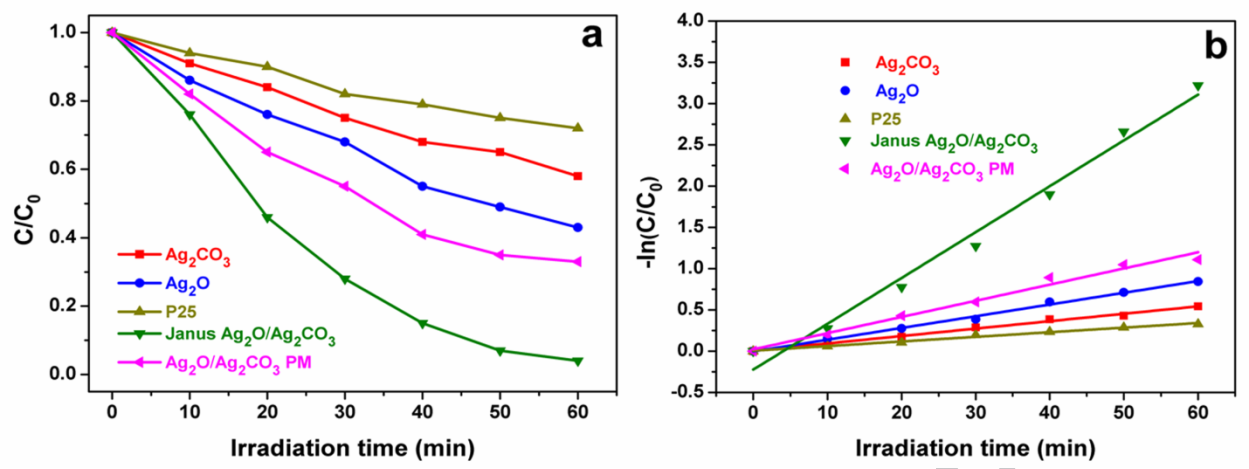

Fig. 5. (a) Comparison of the photocatalytic activities in the decomposition of RhB over the synthesized samples under visible-light illumination, and (b) the related first-order kinetics plots for different samples.

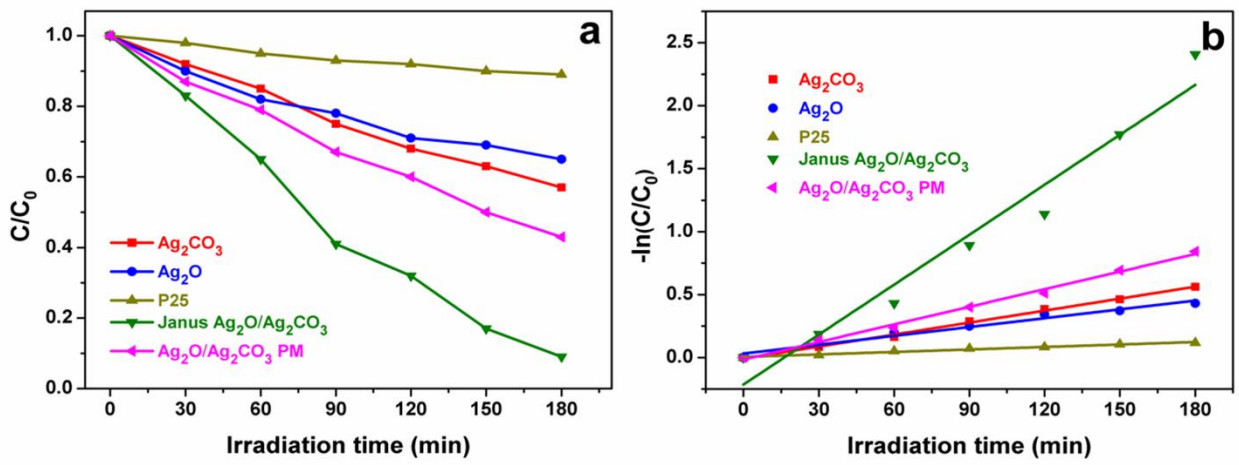

Fig. 6. (a) Comparison of the photocatalytic activities in the decomposition of 4-CP over the synthesized samples under visible-light illumination, and (b) the related first-order kinetics plots for different samples.

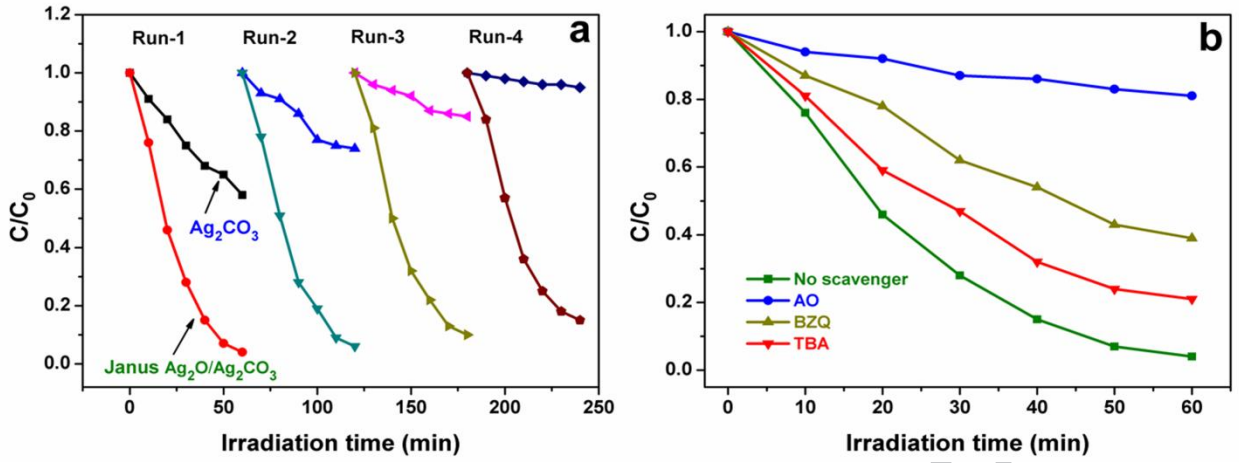

Fig. 7. (a) Reusability of the Janus Ag_2O/Ag_2CO_3 nanocomposite for the degradation of RhB upon visible-light over four successive experimental runs. (b) Effects of different scavengers on the degradation of RhB upon visible-light in the presence of the Janus Ag_2O/Ag_2CO_3 nanocomposite.

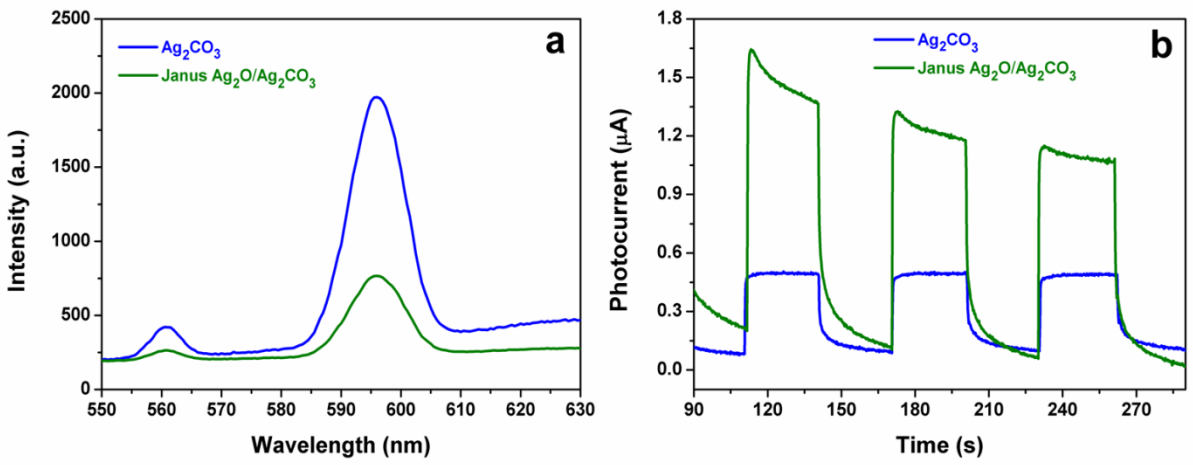

Fig. 8. (a) Time resolved PL patterns and (b) Photocurrent responses of bare Ag_2CO_3 and Janus Ag_2O/Ag_2CO_3 nanocomposite.

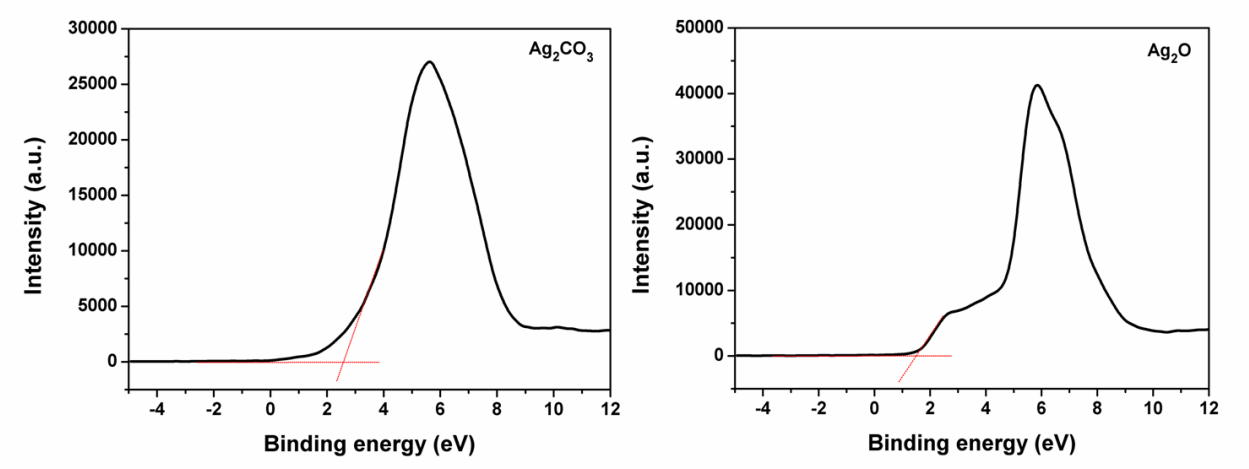

Fig. 9. Valance band XP spectra of bare Ag_2CO_3 and Ag_2O samples.

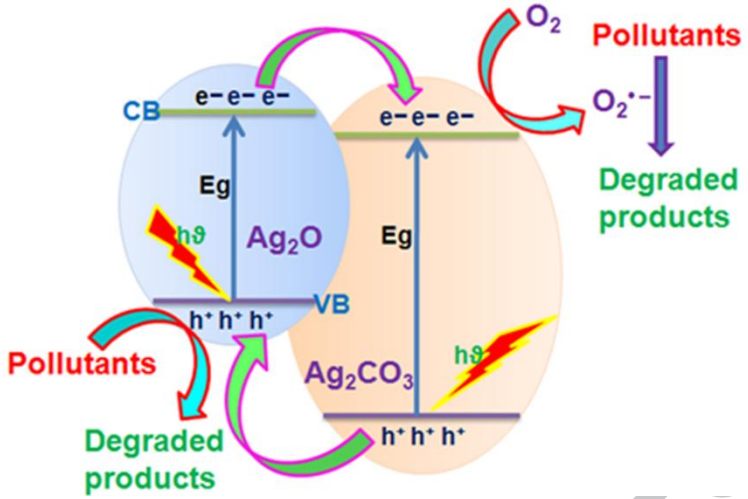

Fig. 10. Schematic illustration of the charge transfer and separation in the Janus Ag_2O/Ag_2CO_3 heterojunction system under visible-light illumination.

Graphical abstract

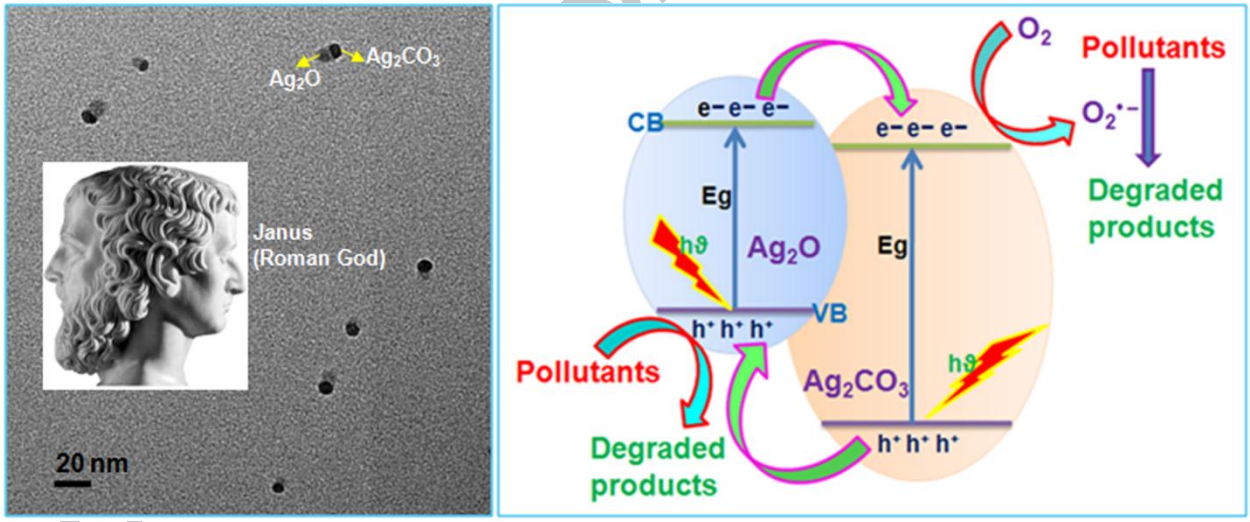

Highlights

- A Janus system was constructed without the need for conventionally used surfactants
- Facile ion-exchange followed by an in situ phase transformation method was used
- Rapid charge transfer at Ag_2O/Ag_2CO_3 interface contributed to enhanced activity
- Janus nanocomposite exhibited excellent photostability in recycling experiments

- Janus system prepared using less harmful chemicals showed high photoactivity